LASER INTERFEROMETER GRAVITATIONAL WAVE OBSERVATORY

LIGO Laboratory / LIGO Scientific Collaboration

LIGO–T060272–00–I *ADVANCED LIGO* 06/11/19

Length Sensing and Control for AdLIGO

Kentaro Somiya, Osamu Miyakawa, Peter Fritschel, and Rana Adhikali

Distribution of this draft:
LIGO Science Collaboration

This is an internal working note
of the LIGO Project.

California Institute of Technology
LIGO Project - MS 18-34
Pasadena, CA 91125
Phone (626) 395-2129
Fax (626) 304-9834
E-mail: info@ligo.caltech.edu

Massachusetts Institute of Technology
LIGO Project - NW17 - 161
Cambridge, MA 01239
Phone (617) 253-4824
Fax (617) 253-7014
E-mail: info@ligo.mit.edu

LIGO Hanford Observatory
P.O. Box 1970
Mail Stop S9-02
Richland, WA 99352
Phone (509) 372-8106
Fax (509) 372-8137

LIGO Livingston Observatory
P.O. Box 940
Livingston, LA 70754

Phone (225) 686-3100
Fax (225) 686-7189

http//www.ligo.caltech.edu/

Contents

1 Introduction

Advanced LIGO will start its operation in 2011. One big improvement from current LIGO is to change the configuration to a detuned RSE system by adding a signal-recycling mirror. We learned many things through a number of table-top and prototype experiments for AdLIGO all over the world, [1][2][3][4][5][6][7] and a default control scheme that employs two RF sidebands, 9 MHz and 180 MHz, was chosen several years ago. In 2005, however, the 40 m interferometer in Caltech as the final prototype before AdLIGO demonstrated the first operation of the suspended PR-RSE with the same control scheme, [8] and many things turned out, one of which is that quadrant photo-detectors do not work with 180 MHz sidebands as it is too high. The frequency could be sufficiently low if the Schnupp asymmetry length be extended to at least one meter, but the largest length available in the current vacuum chamber is 75 cm, which corresponds to 108 MHz with using the same control scheme; note that the frequency should be a multiple of 9 MHz, the free-spectral range (FSR) of the input mode-cleaner.

One alternative scheme has been proposed in ref. [7]. Although it has been used for a demonstration of a suspended RSE interferometer without power recycling, it must be tested more carefully with a full configuration at the 40 m. Besides, issues that can be checked through simulation must be clarified before the test at the 40 m; noise coupling, offset problem, flexibility of a detune phase, etc.

This report summarizes the work of Length-Sensing-and-Control team in the summer 2006. It contains the review of the RSE control schemes, review of a DC readout scheme and laser noise in RSE, [9] development of a way to evaluate shot-noise-limited control-loop noise, an idea to increase flexibility in detuning, and introduction of a new frequency-domain calculation tool *Optickle*.

2 DC readout and laser noise

2.1 Motivation to use DC readout

It is the 180 MHz sideband in the default scheme that transmits through the dark port and could be used for gravitational-wave signals. However, there is only a very small photodetector is available for such a high frequency modulation, and 180 MHz sideband is not suitable as a reference light to be used for the most sensitive signal extraction. A use of DC readout, [10][11] in which the reference light, or so-called the local oscillator, is provided by utilizing mismatches between the arms, is indispensable with the default scheme, and is already included in the plan. Besides, there are many more practical advantages. Here is the list of those.

- RF sideband frequency can be high (in case of 9-180MHz scheme).
- Output mode-cleaner (OMC) can be with high finesse.
- Oscillator phase noise does not appear.
- Laser noise on the DC local oscillator is lower than that on the RF sidebands.
- Photodetector can be simple.
- Nonstationary shot noise does not appear.

Currently the sensitivity of GEO at high frequencies is limited by oscillator noise, nonstationary shot noise, and detector noise, which shows an importance of changing the readout to DC readout. [12] *The finesse of the OMC* will be limited by its optical loss that decreases signals and by displacement noise of the OMC that couples with the offset light, [13] but it is much higher than the finesse of an OMC with RF readout that needs to transmit RF sidebands together with signals. *Oscillator phase noise* is not a problem if the upper and lower RF sidebands are perfectly balanced since noise acts differentially and is cancelled between them, but it becomes a problem as the RF sidebands are highly unbalanced due to the fact that only one of them resonates in the SRC to make a detuned situation for the carrier light. *Laser noise problem*[1] that is recognized and analyzed in ref. [3] and completed in ref. [9] will be briefly explained in this section. *The simplification of the photodetector* will be realized by having no RF components or higher-order spatial modes that would require complicated filter circuits. What should be detected are gravitational-wave signals with TEM00 contrast defect light and TEM00 offset light, and nothing else. *Nonstationary shot noise* can be removed and quantum-noise level can be in the same level with RF readout if a readout quadrature is fixed, [14][15] but it requires higher-order harmonics of the RF sideband appropriately transmitting through the dark port, which is challenging in practice. Nonstationary shot noise results from vacuum fluctuation at the double frequency of the modulation and apparently does not appear with DC readout.

There are also a few challenging factors in a use of DC readout, which are to be tested and hopefully solved at the 40 m experiment very soon. Here is the list. Maybe there are more.

- Direct coupling of acoustic noise.
- Direct coupling of laser intensity noise.
- RF sidebands should be removed at the OMC.
- Severe requirement to the OMC alignment.
- Scattering light problem.

Acoustic noise coupling will become a severe problem. For example, motion of the photodetector in the case with RF readout is not a problem since fluctuation of the local oscillator appears only at the double frequency, but it is a problem with DC readout since the double frequency is still in the observation band. The photodetector should be inside the vacuum chamber. *Intensity noise* also appears by the same logic. On the other hand, as is mentioned in the last paragraph, laser noise on the DC light is lower than that on RF sidebands (see Sec. 2.2). *RF sidebands should be removed* at the OMC to avoid additional shot noise, but they may remain at the dark port since the finesse of the OMC is limited to $500 \sim 1000$. The modulation depths of two pairs of RF sidebands should be as low as possible and also the ratio should be optimally chosen with a consideration of the fact that one of the sidebands transmits through and the others have only a fraction at the dark port. *Tilt of the OMC* may be the hardest one at the use of DC readout. It leads to fluctuation of transmittance of the OMC, which cannot be isolated from gravitational-wave signals. This is one big issue that should be solved by the Alignment-Sensing-and-Control team. *Scattering light* is another problem. There will be a window between the OMC + photodetector chamber and the SRM chamber to allow us to open the latter one more frequently. A fraction of the local oscillator light will be reflected, or scattered, back to the interferometer and will impose noise.

[1] Probably this problem was the primary motivation to employ DC readout at the beginning.

2.2 Laser noise and readout quadrature

Figure 1 shows light fields at the dark port of PRFPMI with RF readout that contribute to frequency noise or intensity noise. In the phasor diagram, only light fields that are parallel to each other generate noise at the photodetection, and the cross terms between RF-RF or DC-DC are filtered out at the demodulation process. It is frequency noise on RF sidebands coupled with contrast defect[2] that makes the biggest contribution since frequency noise on the carrier light is filtered out by the power-recycled arm cavity. The RF sidebands also experience the filtering but the cavity pole of the power-recycled Michelson interferometer is higher than the observation band. Similarly, it is intensity noise on the RF sidebands coupled with an rms fluctuation component that appears as intensity noise in total.

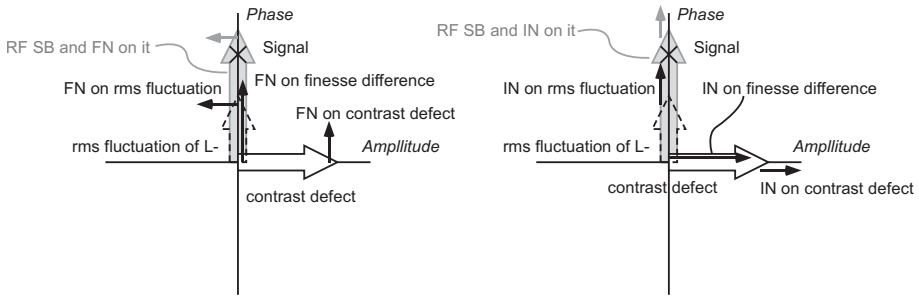

Figure 1: Phasor diagram of the light field at the detection port with the RF readout scheme. Left panel shows DC components and audio sidebands of frequency noise. Right panel shows DC components and audio sidebands of intensity noise.

Apparently it is reasonable to replace RF sidebands to a carrier light that can appear at the dark port with some microscopic offset length to the L_-. RF sidebands are filtered out by the OMC and only the offset light and the contrast defect light come out to the signal extraction port as DC components. This DC readout scheme will be used also in middle LIGO. Laser noise is lower than that with RF readout. [9][11] The readout quadrature can be changed from $\zeta = 0$, which is the phase quadrature of PRFPMI, so that quantum radiation pressure noise be reduced, [16] but it is not essential in middle LIGO.

Laser noise of AdLIGO in the readout quadrature of $\zeta = 0$ and $\pi/2$ is shown in Fig. 2 (top). Definition of the detune phase and the readout quadrature follow the definition in ref. [17]. It is still true that laser noise on the carrier is filtered out, but the difference is more dramatic because the readout quadrature is not same between the RF and DC readout schemes. As is shown in Fig. 2 (bottom), the remained carrier light consists of the contrast defect together with an offset light caused by radiation pressure of the contrast defect light that reflects back into the interferometer through the signal-recycling mirror. With RF readout, the feedback servo will suppress the total output in the readout quadrature, so finally the carrier light remains in the quadrature that is 90 deg different from ζ. With DC readout, on the contrary, the quadrature of the remained carrier light corresponds to the readout quadrature ζ.

In the case of AdLIGO, the readout quadrature alters the shape of the sensitivity curve. The sensitivity at the optical spring frequency could be better with $\zeta = 0$, but thermal noise will limit

[2]Note that contrast defect here only means the field due to loss imbalance.

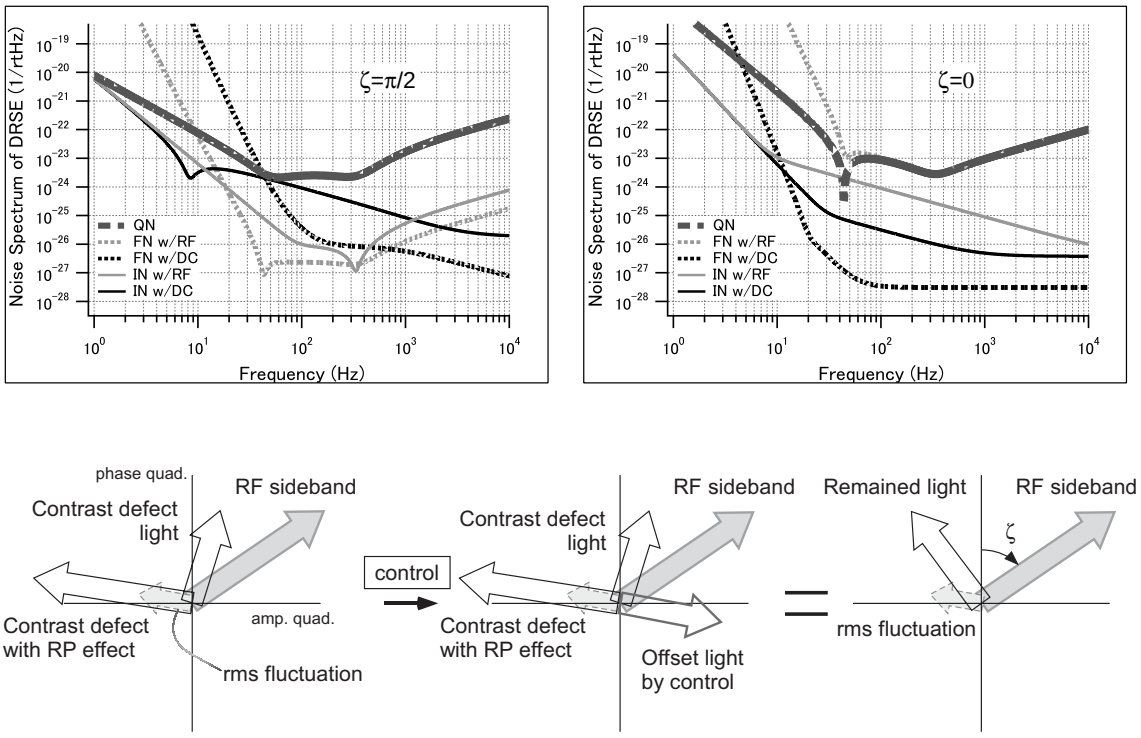

Figure 2: *Top panel:* Quantum noise and laser noise in two different readout quadratures. *Bottom panel:* DC components of the carrier light and the RF sidebands at the dark port of the RSE interferometer. The offset light caused by radiation pressure of the reinjected contrast defect light can be suppressed by the control system.

the sensitivity at around the frequency. The sensitivity at low frequencies is better with $\zeta = \pi/2$, which is important for gravitational waves from binary inspiral events, one of the primary targets of AdLIGO.

Now it turns out that the best quadrature for gravitational waves is the worst quadrature for laser noise. But it is not a problem. Figure 3 shows that a quantum noise curve does not change its shape much while laser noise goes sufficiently below the sensitivity in the observation band if we choose the readout quadrature to be -78 deg. Here losses are included and laser noise is derived with frequency and intensity stabilizations up to a shot-noise level of 1 W light. It is frequency noise, coupling with rms fluctuation of the arms, reflecting back through the SRM and shaking the mirrors by radiation pressure, that makes the biggest contribution of all laser noise components. Laser noise spectrum changes a little bit with $\zeta = +78$ deg, while quantum noise curve is same.

Let us see how much offset light we need to realize the readout in $\zeta = -78$ deg. According to ref. [9], the DC component of the carrier light is given as

$$\begin{pmatrix} B_1 \\ B_2 \end{pmatrix}_{\rm RSE} = \frac{g_{\rm pr} E_0}{2\sqrt{2}} \begin{pmatrix} \dfrac{\tau\xi(1-\rho)\cos\phi}{M_{\rm free}} - \dfrac{\tau(1+\rho)\sin\phi}{M_{\rm free}} \dfrac{2\omega_0 \Delta L_{\rm D}}{L\omega_{\rm c}} \\ \dfrac{\tau\xi(1+\rho)\sin\phi}{M_{\rm free}} + \dfrac{\tau(1-\rho)\cos\phi}{M_{\rm free}} \dfrac{2\omega_0 \Delta L_{\rm D}}{L\omega_{\rm c}} \end{pmatrix} , \tag{1}$$

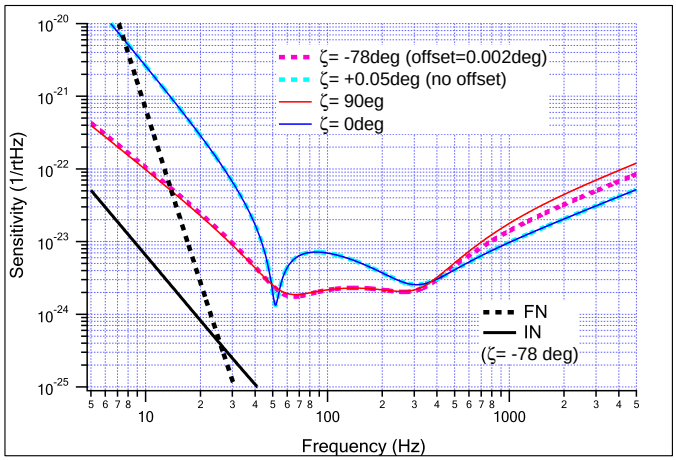

Figure 3: Quantum noise of AdLIGO with different readout phase. Blue and red curves are with nominal readout phases that are usually shown in papers. DC readout with the offset to L_- up to 0.002 deg allows us to choose ζ between -78.06 and +0.05 deg, spectra with which are shown in sky-blue and purple curves, respectively. Laser noise with $\zeta = -78$ deg is also shown.

where, ρ and τ are reflectivity and transmittance of the signal-recycling mirror, ξ is a contrast defect factor described by a transmittance of the carrier light from the bright port to the dark port, ϕ is a detune phase, ω_0 is the angular frequency of laser light, L is arm length, ΔL is the actual differential offset length, and

$$M_{\rm free} = 1 + \rho^2 - 2\rho\cos 2\phi \tag{2}$$

expresses susceptibility of the free mass interferometer; one might have seen M with the optical spring in ref. [17]. The upper and lower column represents amplitude and phase quadrature, respectively. For example, with $\rho = 0$, $\tau = 1$, and $\phi = 0$, which makes a simple Fabry-Perot Michelson interferometer, eq. (1) shows a contrast defect term with ξ in the amplitude quadrature B_1, and an offset term with ΔL in the phase quadrature, which makes sense. The readout quadrature with DC readout is then

$$\zeta_{\rm DC} = \arctan\left(\frac{B_1}{B_2}\right). \tag{3}$$

Replacing the offset length $\Delta L_{\rm D}$ by the phase $\chi_{\rm d}$, we have

$$\zeta_{\rm DC} = \arctan\left[\frac{\xi(1-\rho)\cos\phi - 8\chi_{\rm d}/T\cdot(1+\rho)\sin\phi}{\xi(1+\rho)\sin\phi + 8\chi_{\rm d}/T\cdot(1-\rho)\cos\phi}\right]. \tag{4}$$

Here the cavity pole is also replaced by the transmittance of front mirrors; $\omega_{\rm c} \simeq Tc/4L$ ($T = 0.005$ in AdLIGO). Contrast defect with 30 ppm loss imbalance results in $\xi = 0.012$, and the optimal detuning for NS-NS binaries is 2.5 deg from broadband RSE, which means $\phi = \pi/2 - 0.08$. The

offset that makes $\zeta = -78$ deg is derived to be $\chi_{\rm d} = 0.002$ deg (or $\Delta L_{\rm D} \simeq 5.9 \times 10^{-12}$ m):

$$\chi_{\rm d} = 0.002 \Longleftrightarrow \zeta_{\rm DC} = -78.06 \text{ deg} . \tag{5}$$

Photodetectors will be able to receive the light up to 100 mW, and the offset of $\chi_{\rm d} = 0.002$ deg results in ~ 79 mW light in total at the dark port, which is acceptable. If no offset is added to the differential arm length, while the radiation pressure offset is suppressed, then

$$\chi_{\rm d} = 0 \iff \zeta_{\rm DC} = +0.05 \text{ deg} . \tag{6}$$

The summary of this section follows: Readout quadrature should be chosen

- to obtain a good sensitivity to binary inspiral events ($\zeta \sim \pm 90$ deg),
- not to let laser noise limit the sensitivity above ~ 20 Hz ($\zeta > -78$ deg),
- not to have total light more than 100 mW at the dark port,

and we choose the answer.

3 Double modulation and asymmetry optimization

3.1 High contrast between two RF sidebands

The signal extraction of L_- will be achieved with DC readout, but the other degrees of freedom will be measured with a modulation-demodulation scheme. One difference from initial LIGO is that there will be two modulation frequencies. In addition to L_+ and ℓ_+, the signal-recycling cavity length ℓ_s should be controlled in AdLIGO. Since all the three motions appear as I-phase signals (phase modulation common to the upper and lower RF sidebands or phase modulation to the carrier light), taking independent signals from the bright port (BP) and the pick-off port (PO), like we do in initial LIGO, is not enough. We use f_1 and f_2 sidebands. A beat signal between the carrier light and one of the sidebands is used for L_+ signal, and beat signals between two sidebands at different ports are used for ℓ_+, ℓ_-, and ℓ_s signals without being disturbed by large $L_\pm$ signals. If there are sidebands of sidebands, or sub-sidebands, at a detection port, $L_\pm$ signals appears at the same frequency as the beats between f_1 and f_2 sidebands, and will contaminate ℓ signals, so we cannot locate two EOMs in series. Either to add up two carrier lights with each modulation using a Mach-Zehnder interferometer [18][19][20][21] or to eliminate sub-sidebands by additional modulations combined with an optimal proportion [7][36][22] is necessary. In this report, we assume no sub-sidebands anywhere. Simulation tools like FINESSE or Optickle does not have sub-sideband effect in default settings.

Now let us see what is the best combination of two pairs of sidebands to control ℓ_+, ℓ_-, and ℓ_s; or the central dual-recycled Michelson interferometer (DRMI). One point is that we need to isolate ℓ_+ and ℓ_s that can be identical. Figure 4 shows a good comparison between the isolation of L_+ and ℓ_+ in PRFPMI and possible isolation of ℓ_+ and ℓ_s in DRMI. In the left panel, assuming the MI reflectivity for a sideband is equal to the PRM reflectivity (critical coupling), which makes the sideband transmit through the dark port, we can avoid to have L_+ at BP as there is no local oscillator light that can couple with the carrier signal. On the other hand, the output at PO mainly contains L_+. Consequently the proportion of the two signals can be quite different between the

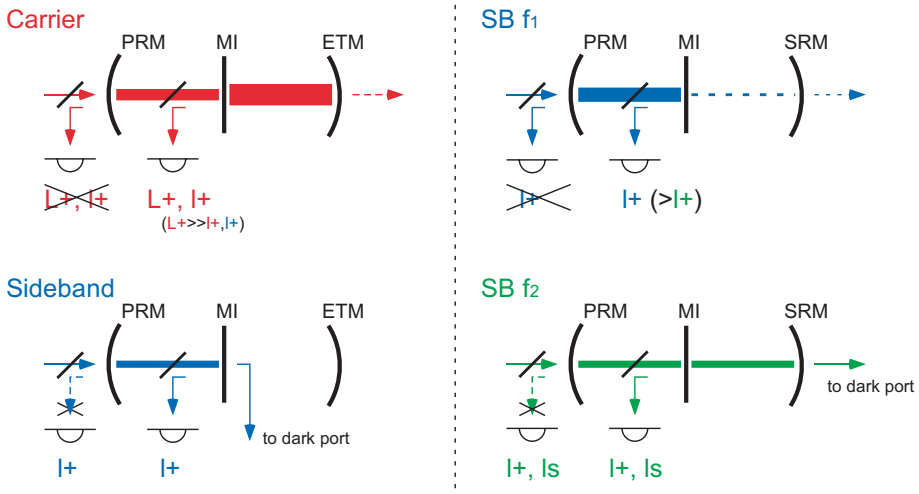

Figure 4: Similarity between the isolation of ℓ_+ from L_+ in PRFPMI and the isolation of ℓ_+ and ℓ_s in DRMI.

outputs at BP and PO. The same thing can be done with DRMI. If f_1 sideband does not resonate in the SRC, and f_2 sideband does resonate in the SRC with the critical coupling between PRM and SRMI, a ℓ_+ signal that f_1 sideband brings to BP has no local oscillator to couple with, and it is only a ℓ_+ signal of f_2 that remains in the output at BP. On the other hand, the output of PO contains both ℓ_+ signals probed by f_1 and f_2. They cancel each other but since the finesse of the PRC is higher for f_1 due to the non-resonance of the SRC, ℓ_+ of f_1 is dominant at PO. Consequently, although there are both ℓ_+ and ℓ_s at BP and PO, ℓ_+ signals obtained at the two ports have opposite signs with respect to ℓ_s at each port. Of course this is a very optimal situation, but the basis of signal separation lies on this concept.

The critical coupling for f_2 sideband can be done in several ways. See Fig. 5. In the default plan of AdLIGO (9-180), for f_2 sideband, the PRC is anti-resonant, the asymmetry of MI is $\alpha = \pi/2$, and the SRM is resonant. In the 40m (33.2-166), the PRC is resonant, the asymmetry is $\pi/2$, and the SRM is anti-resonant. The transmittance of MI is $(i \sin\alpha)^2 = -1$ and the reflectivity of two recycling mirrors are equal, so this three-mirror coupled cavity system is in critical coupling for f_2 sideband. Indeed it is like a single cavity as the middle mirror has no reflectivity. It is also possible to maintain the critical coupling even if each recycling cavity is detuned for f_2 by same amount with opposite sign. [23]

However, $\alpha = \pi/2$ leads to the fact that the frequency of f_2 sideband needs to be high with a fixed asymmetry length $\Delta\ell$:

$$\alpha = \frac{\Delta\ell\omega_{\rm m}}{c} \,. \tag{7}$$

One way to have this asymmetry α small with f_2 sideband being still in critical coupling in DRMI is to make both PRC and SRC resonant for f_2 sideband. The reflectivity and transmittance of SRMI

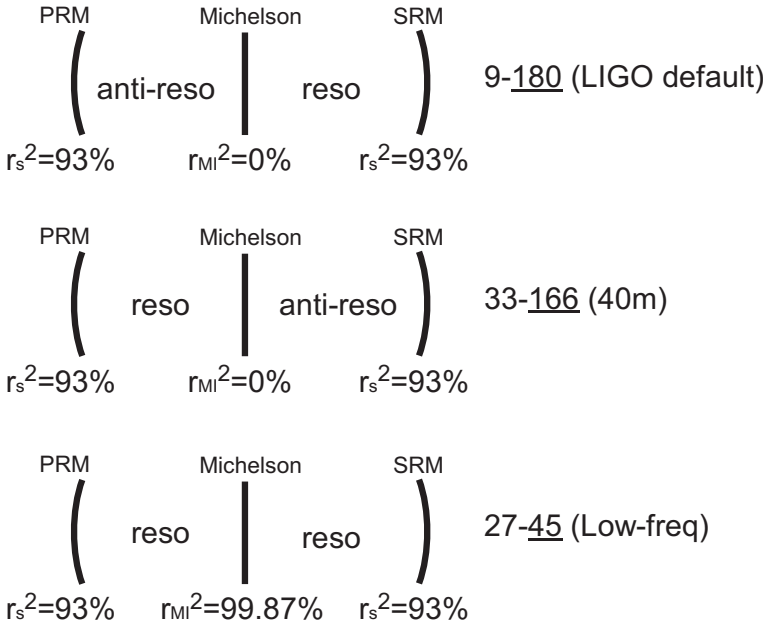

Figure 5: Three different ways to realize critical coupling in the DRMI.

in resonance is given by

$$r_{\rm SRMI} = \cos\alpha - \frac{r_s \sin^2\alpha}{1 - r_s\cos\alpha} \qquad ({\rm BP} \to {\rm BP \ or \ DP} \to {\rm DP}) \,, \tag{8}$$

$$t_{\rm SRMI} = t_s \left[\frac{i\sin\alpha}{1 - r_s\cos\alpha}\right] \qquad ({\rm BP} \to {\rm DP \ or \ DP} \to {\rm BP}). \tag{9}$$

The critical coupling is realized with $r_p = r_{\rm SRMI}$, which reads

$$\cos\alpha = \frac{r_p + r_s}{1 + r_p r_s} \,. \tag{10}$$

Here the amplitude reflectivity r_p for PRM or r_s $(= \rho)$ for SRM is positive with the resonance of each recycling cavity, and is negative with the anti-resonance. One can see Eq. (10) has two solutions. One is with either of recycling cavities being resonant, which means the signs of r_p and r_s are opposite, and the other is with both recycling cavities being resonant. Note that $|r_p| = |r_s|$ in AdLIGO. Then the former solution requires

$$\alpha = \frac{\pi}{2} \quad ({\rm HF \ solution}) \,, \tag{11}$$

and the latter requires

$$\begin{aligned} \alpha &= \arccos\frac{\sqrt{0.93} + \sqrt{0.93}}{1 + \sqrt{0.93}\sqrt{0.93}} \\ &= 0.036\,{\rm rad} \quad ({\rm LF \ solution}) \,. \end{aligned} \tag{12}$$

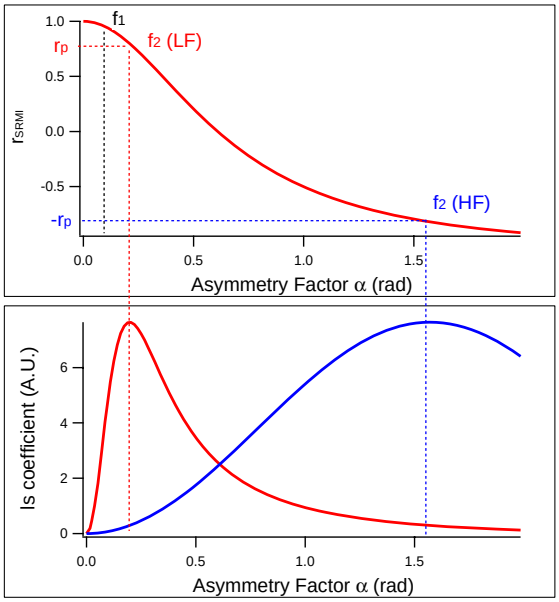

Figure 6: The coefficient of ℓ_s signal is maximized when the reflectivity of SRMI matches to $\pm r_p$. Asymmetry being optimized with f_2, the coefficient is also large in the LF scheme if f_1 is in resonance.

Using 45 MHz for f_2 with the LF solution, we have $\Delta\ell = 3.85$ cm. The length becomes longer with optical losses taken into account, but still it is much shorter than that with the HF solution. There are a couple of differences between the HF and LF schemes in the lock acquisition process. One is that the DRMI in the LF scheme is a 3-mirror coupled cavity while that in the HF scheme is a single cavity. The reflectivity of MI being high may makes a difficulty, which should be checked at the 40 m experiment, but the performance is same after everything is locked. The other difference is that f_1 could resonate in DRMI with a reasonably high robustness since f_1 frequency and f_2 frequency are closer than the HF scheme. See Fig. 6 and its caption. This difference will be discussed in Sec. 4.

There are many beneficial points with DRMI being in the critical coupling or close to it. One is that the efficiency to obtain ℓ_s signal is maximized. Amplitude reflectivity of DRMI for f_2 sideband with a phase shift ψ_s due to the motion of SRM is given by

$$r_{\rm DRMI} \simeq -r_p + \frac{t_p^2[(\cos\alpha - r_s)(1 + r_p r_s - (r_p + r_s)\cos\alpha) + i r_s \sin^2\alpha \cdot \psi_s]}{[1 + r_p r_s - (r_p + r_s)\cos\alpha]^2}\,, \qquad (13)$$

where, with the critical coupling condition Eq. (10), the coefficient of ψ_s is maximized at BP.

Here is the list of benefits provided by the high contrast between two RF sidebands due to the critical coupling of f_2 in DRMI.

- Extraction of independent ℓ_+ and ℓ_s signals at BP and PO,
- Maximization of ℓ_s signal at BP,
- Moderation of an offset problem at BP (see Sec. 5).

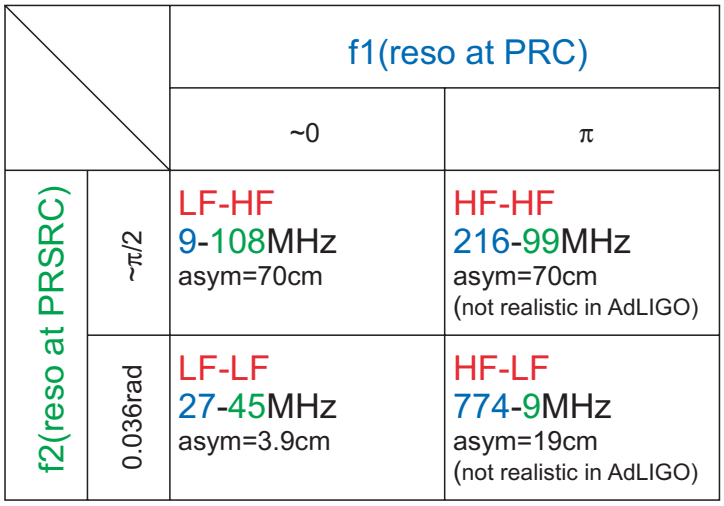

Figure 7: There are 4 different ways to choose the sideband frequencies.

The followings are miscellanies thoughts related to this section. *Most of them have nothing to do with AdLIGO*.

3.2 Misc-1 : Categorize the control schemes

We have seen that there are two ways to choose an f_2 frequency, while f_1 is fixed to a frequency just as low as possible in order to have little f_1 at DP. A leak of f_1 to DP causes not only a contamination of the contrast between two sidebands but also an undesirable imbalance between the upper and lower f_1 sidebands as the SRC is detuned in AdLIGO (see Sec. 4). The lowest frequency for f_1 in AdLIGO is 9 MHz, which is the FSR of the input MC. With this number being fixed, f_1 with the LF scheme will leak less to DP than that with the HF scheme since the asymmetry length is shorter. In fact, the leak could be zero if f_1 frequency is changed so as to make the asymmetry α be π. This is the way used in the table-top experiment in University of Florida, [2] and also the way planned to use in LCGT with α being 3π instead of π. [23]

Now we can categorize RSE control schemes into four; LF and HF for f_1 and f_2. [24] See Fig. 7. While the asymmetry of the LF-HF scheme can be tuned to realize the critical coupling for f_2, which can be slightly different from $\pi/2$ depending of losses, that of the HF-HF scheme should be tuned to realize perfect reflectivity for f_1; the critical coupling is not so restrictive. The f_1 frequency in the HF-HF scheme or in the HF-LF scheme is too high in AdLIGO, while this is applicable in LCGT that has lower reflectivity of the SRM.

3.3 Misc-2 : Discussion about ℓ_- signal

Considering the efficiency of ℓ_- signal, we have recently found one strong point of the HF-LF scheme, although it is not applicable to AdLIGO. To avoid increase of a shot-noise level of ℓ_-,

the signal should be obtained at DP, more specifically the reflective port of the OMC. While L_- signal, which is also obtained at DP, is almost in anti-resonance in the SRC, ℓ_- signal around the f_1 sideband frequency could be in resonance in the SRC so that the signal can increase at the observation frequencies. However, this is not allowed in the LF-LF or LF-HF scheme since it makes f_1 sideband, which is supposed to reflect back to BP, transmit to DP. In the HF-HF scheme, f_1 sideband does not leak through DP except for ℓ_- components, but there is no combination of f_1 and f_2 frequencies that satisfies necessary conditions. Meanwhile the HF-LF scheme has a solution with $\alpha = 2\pi$ instead of π. Unfortunately, this idea cannot be used in AdLIGO anyway.

In fact, it turns out that ℓ_- signal can be signal-recycled in the PRC. More discussions about ℓ_- will be made in Sec. 6.3.

4 Detuning and its flexibility

4.1 Sideband locking

A detuned situation can be realized if twice the modulation frequency is so far from the multiple of the FSR that the detuning is more than one line width from resonance; roughly $T_s/4 \ll \Delta\psi_s$. When the detuning is smaller than this limit, each error signal from the upper and lower sideband produces an offset that cancels each other. Then both sidebands are locked to a slightly non-resonant condition[3] and the carrier is locked to either resonance or anti-resonance (Fig. 8). When the detuning is larger than this limit, either the upper or lower sideband comes to resonate and produces the error signal while the other sideband produces almost no signal. Then the carrier is locked to a detuned condition.

In the PRC the carrier is locked to the anti-resonance in the cavity even if the FSR is slightly different from what it should be. In the SRC, as far as the detune phase is bigger than 1 deg, the SRC is locked to the resonance of one of sidebands. If we want a slight detuning, we should not use the sideband-locking but the usual carrier-locking with adding a DC offset to the error signal. The dune phase of AdLIGO, optimized to NS-NS binaries, is 2.5 deg from the tuned RSE, which is appropriate for the sideband-locking.

Figure 9 shows the parameters used in FINESSE for 27-45 MHz scheme as an example. Both upper and lower f_1 sidebands should resonate in the PRC and not resonate in the SRC, and the upper sideband of f_2 should resonate in the PR-SRC; it seems that the other way results in a negative optical spring. The FSR of the PRC, which should be anti-resonant for the carrier light, is $2f_1 = 18$ MHz, thus

$$\mathrm{PRC\ length} \rightarrow \frac{c}{4f_1} = 8.32757\,\mathrm{m}. \tag{14}$$

The FSR of the SRC is given as

$$\mathrm{SRC\ length} = \frac{c}{2f_2}\left(\frac{(2n+1)\pi - 2\phi}{2\pi}\right) \tag{15}$$

where ϕ is a detune phase and n is integer that should be chosen not to let 27 MHz resonate.

[3] This is called *delocation* in ref. [23]. It is used to change the balance of signal appearance at each port.

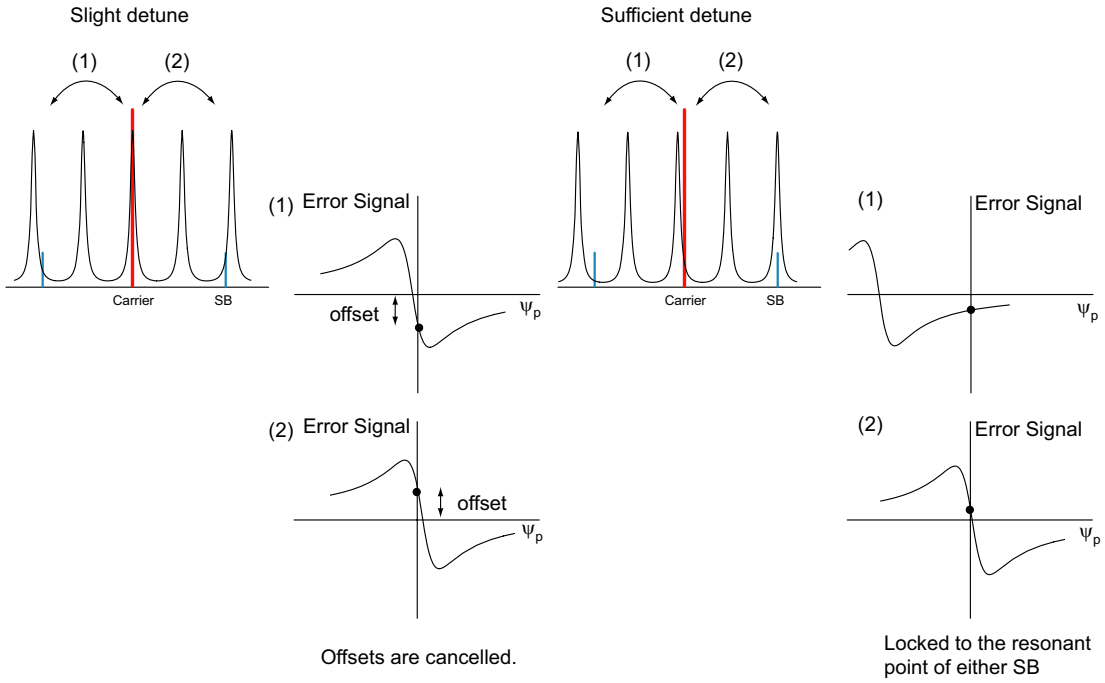

Figure 8: The carrier is locked to the resonance (tuned RSE) if the detuning is slight (left). The carrier is locked to a detuned condition only if the SRC length is sufficiently detuned (right).

Choosing $n = 1$ and detune phase $\phi = \pi/2 + 0.044\,\mathrm{rad} = 92.5\,\mathrm{deg}$, we will have

$$\mathrm{SRC\ length} \rightarrow 3.28461\mathrm{m}. \tag{16}$$

Note that the definition of detune phase is different from reference [17], where $\phi_{\mathrm{BC}} = \pi - \phi$. The asymmetry length $\Delta\ell$ to make the critical coupling for 45 MHz sideband is given from Eqs. (7) and (10) as

$$\Delta\ell = 0.0362774 \times \frac{c}{\omega_{\mathrm{m}}} = 0.0384649\,\mathrm{m}. \tag{17}$$

The numbers shown in Fig. 9 have been manually tuned to maximize the transmittance of the RF sidebands, and are slightly different from what are analytically derived here because of optical losses. The lengths of the recycling cavities should be chosen to be suitable for the vacuum system of AdLIGO, which can be either around 8 ± 1 m, around 23 ± 2 m, or around 53 ± 4 m[4].

4.2 Alternative operation point

The detune phase is almost fixed to what is determined by a macroscopic length of the SRC and a sideband frequency. One could slightly change the phase by adding offset to the error signal

[4]There are two vacuum chambers both at BP and DP. If we use the closer chamber, the recycling cavity length will be around 8 m, and if use the further one, the length will be around 23 m. We might extend the length in order to obtain better signal for alignment control, in which case the recycling cavities will be folded and the length becomes ~ 53 m.

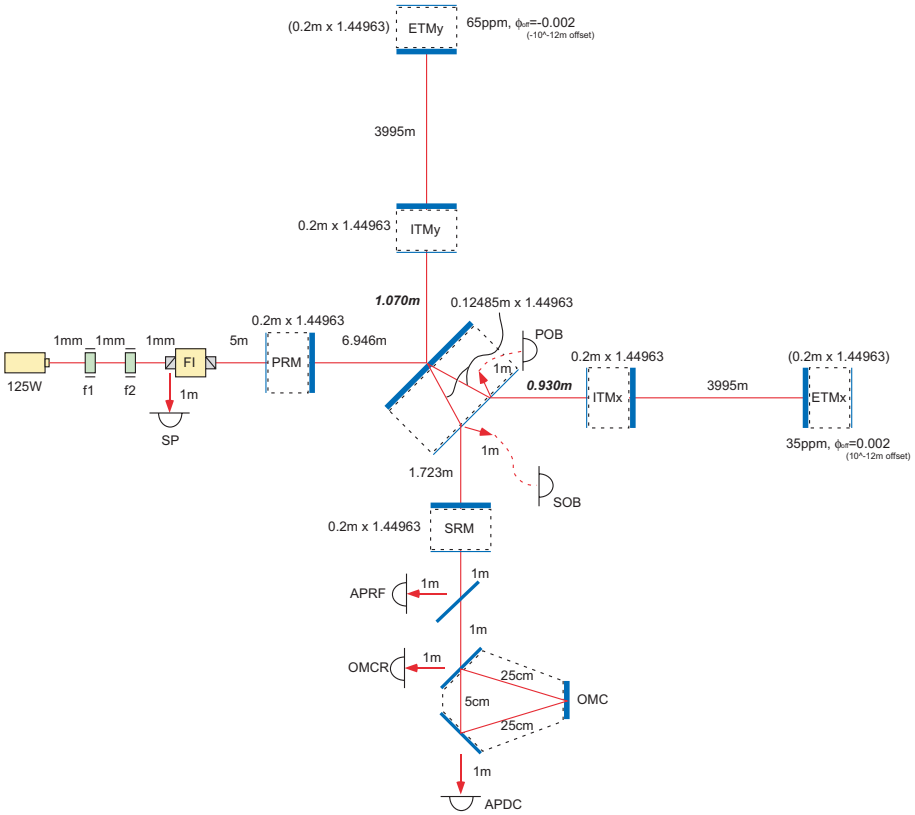

Figure 9: AdLIGO length parameters used in FINESSE for the LF-LF control scheme. The asymmetry (shown in bold letters) has been tuned to maximize one of the f_2 sidebands transmitted to AP. There are two pickoff ports from the AR coating of the beamsplitter.

of ℓ_s, but it is only $\sim$ 1 deg around the fixed detune phase. Figure 10 shows quantum noise curves whose parameters are optimized to NS-NS binaries (red curve) and BH-BH binaries (blue curve), with estimated classical noise curves. Incident laser power and a detune phase for the red curve are $I_0 = 125$ W and $\phi = 90 - 2.5$ deg, and those for the blue curve are $I_0 = 5$ W and $\phi = 90 - 14$ deg. [25] The merger frequency for $30M_\odot - 30M_\odot$ BH binaries is ~ 70 Hz, so the sensitivity above this frequency has nothing to do with the observation.

Let us see if we can have two alterable operation points with detune phases that are optimal for NS-NS binaries and BH-BH binaries. As we have mentioned in Sec. 3.1, f_1 sideband with the LF scheme can resonate in the SRC instead of f_2 sideband. Using Eq. (15), we have

$$\text{FSR of SRC} = \frac{c}{2L_\mathrm{s}} = \pi \times \frac{f_1}{n_1\pi - \phi_1} = \pi \times \frac{f_2}{n_2\pi - \phi_2}\,, \tag{18}$$

where integer n_i is the number of resonant points between the carrier and the sideband, L_s is the SRC length, f_i (i =1 or 2) is the RF-sideband frequency, and ϕ_i is the detune phase with one of

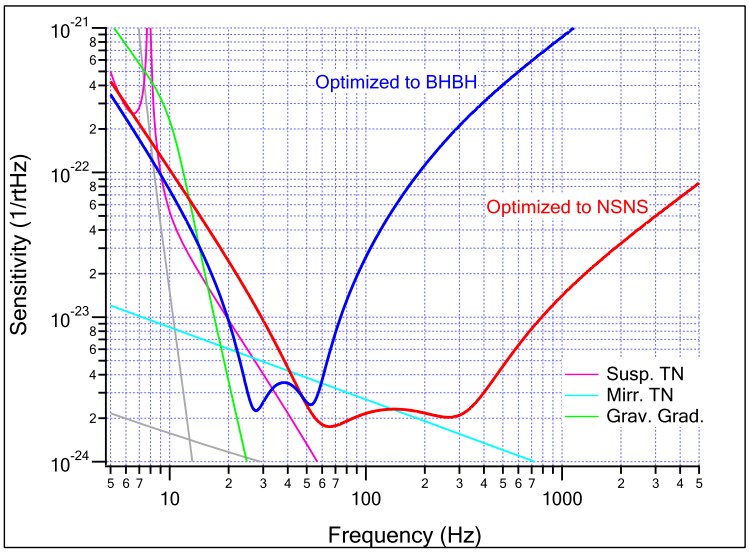

Figure 10: Quantum noise curve with the laser power and the detune phase optimized for gravitational waves from NS-NS or BH-BH binaries, and other classical noise estimated with AdLIGO parameters. Quantum noise curves may be slightly different from what are shown in ref. [25] since here the readout quadrature is fixed to -78 deg and also losses may be different.

the $\pm f_i$ sidebands being resonant in the SRC. From Eq. (18), we have

$$\phi_1 = \frac{n_2\pi f_1 - \phi_2 f_1 - n_1\pi f_2}{f_2} \,. \tag{19}$$

The sideband frequencies in the LF scheme are odd multiples of 9 MHz. Being careful not to make $f_1 + f_2$ higher than 100 MHz, we have several candidates that are combinations of 9, 27, 45, and 63 MHz. Let us fix ϕ_2 to $90 - 2.5$ deg and look for ϕ_1 that is close enough to $90 - 14$ deg. Note that we do not need to follow $f_1 < f_2$.

Finally the best solution[5] is $\phi_2 = 12.5$ deg with $f_1 = 45$ MHz, $f_2 = 9$ MHz, $n_1 = 73$, $n_2 = 15$, and $L_s = 49.8$ m. So we shall pick 45-9 MHz scheme as one hopeful candidate for the AdLIGO control scheme. More flexibility can be obtained with a use of two polarization beams, which is introduced in Appendix. B.

5 Double demodulation and offset problem

5.1 Original purpose of double demodulation

Beat signals between two sidebands will be obtained by double demodulation. The output of a photodetector is demodulated by either f_1 or f_2 first, then is demodulated again by the other frequency. It is equivalent to demodulate the output by $f_1 + f_2$ and $f_1 - f_2$ and add them up. Indeed, the latter way is used at the 40 m. Single demodulation generates two different kinds of

[5]The second best is $\phi_2 = 17.5$ deg with $f_1 = 63$ MHz and $f_2 = 9$ MHz.

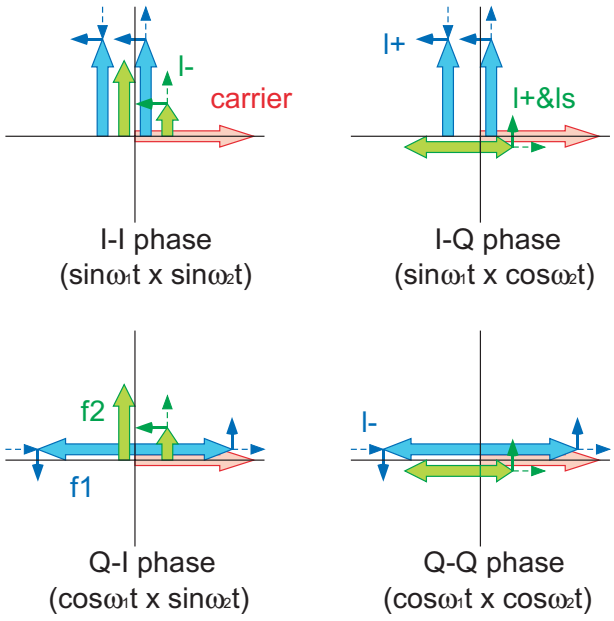

Figure 11: Phasor diagrams that express 4 different phases of a double-demodulation output at the bright port of AdLIGO. At the pick-off port, the balance of the upper and lower f_2 sidebands is the other way and the sign of ℓ_+ signal obtained from I-Q-phase flips. The most important point here is that only the I-I-phase output has an offset and Q-Q-phase signal cannot be isolated from the offset by a single demodulation by can be by double demodulation.

signal due to the phase of the local oscillator, which are I-phase signal with $\sin\omega_{\rm m}t$ and Q-phase signal with $\cos\omega_{\rm m}t$. Double demodulation generates four kinds of signal, which correspond to I-I-, I-Q-, Q-I-, and Q-Q-phase signals. If one uses the single demodulation by either of $f_1 \pm f_2$, I-I- and Q-Q-phase signals are mixed and appear as a Q-phase signal and I-Q- and Q-I-phase signals appear as an I-phase signal.

Interestingly, in ref. [26], it is only at the signal extraction of ℓ_- when the double demodulation is planned to use. The reason can be explained in Fig. 11. In a phasor diagram, dc components and ac components are expressed by thick arrows and thin arrows, respectively. Here small letters are used to distinguish dc ($\leftrightarrow$ ac) from DC ($\leftrightarrow$ RF). This diagram is at BP of AdLIGO and we assume that f_1 sidebands are balanced and f_2 sidebands are highly unbalanced. Note that an ac component can be read out only with a non-zero dc component parallel to the ac component. In I-Q-phase, ℓ_+ on f_1 couples with f_2 dc and $\ell_+ + \ell_s$ on f_2 couples with f_1 dc. In Q-I-phase, no signal can be read out. In Q-Q-phase, ℓ_- on f_1 couples with f_2 dc. Now a problem is I-I-phase, in which it is not only ℓ_- on f_2 that couples with f_1 dc but also f_2 dc couples with f_1 dc that makes an offset. This is the reason why we need the double demodulation; to isolate Q-Q from I-I. One can obtain the ℓ_- signal at DP instead of BP, but will encounter a similar situation.

However, in reality, the offset problem lies not only at the signal extraction of ℓ_- but also at the signal extraction of ℓ_+ or ℓ_s. It may be rather simple to say that the double demodulation is used so that one can eliminate the offset by tuning the first demodulation phase and then maximize the signal by tuning the second demodulation phase. In fact, it is not sure that we should eliminate

the offset or not. The offset can be cancelled out by adding voltage offset to the error signal. Robustness of the control is an issue, but the difficulty is same as the DC readout scheme where we will anyway add a voltage offset. In the following calculations, both demodulation phases are chosen so that a signal of concern can be maximized. If the robustness problem turns out severe, we can still choose demodulation phases to enhance the signal amount under the condition of zero offset. [27]

5.2 Detector noise

Actual trouble that the offset may cause is reduction of detector resolution, which increases detector noise. A typical photodetector we expect to use in AdLIGO will be able to receive light up to 100 mV and generate $\sim 1\ \mathrm{nV}/\sqrt{\mathrm{Hz}}$ noise regardless of input voltage. Assume that we can band-pass filter the outputs at double-demodulation frequencies, then it is a sum of ac signal and dc offset that determines the input voltage. If the offset level exceeds 100 mV, the gain of the photodetector should be reduced, then detector noise, calibrated from Volt to meter, appears more on the sensitivity curve. Detector noise is given by the following equation:

$$\text{detector noise}\ (\mathrm{m}/\sqrt{\mathrm{Hz}}) = \frac{\text{offset}\ (\mathrm{W})}{\text{optical gain}\ (\mathrm{W/m})} \times \frac{1\ \mathrm{nV}/\sqrt{\mathrm{Hz}}}{100\ \mathrm{mV}}\ , \tag{20}$$

while shot noise is described with the same optical gain as

$$\text{shot noise}\ (\mathrm{m}/\sqrt{\mathrm{Hz}}) = \frac{\hbar\omega_0\ (\mathrm{W}/\sqrt{\mathrm{Hz}})}{\text{optical gain}\ (\mathrm{W/m})}\ . \tag{21}$$

Thus, a proportion from total readout noise to pure shot noise is

$$\frac{\text{"detector + shot" noise}}{\text{shot noise}} = \sqrt{1 + \left(\frac{\text{offset}\ (\mathrm{W})}{\hbar\omega_0\ (\mathrm{W}/\sqrt{\mathrm{Hz}})} \times \frac{1\ \mathrm{nV}/\sqrt{\mathrm{Hz}}}{100\ \mathrm{mV}}\right)^2}\ , \tag{22}$$

which we name *d-range factor*. Actually the unit used in the equations does not need to be Watt. FINESSE gives us the offset and the optical gain with a same unit, so we just take the ratio of two and put into Eq. (20).

It is not an offset at a chosen readout phase that determines the d-range factor, but the largest offset in all readout phases. In the ideal case like is shown in Fig. 11, the largest offset comes from I-I-phase. Since the offset is mainly caused by a non-resonant sideband, a use of a single sideband for f_2 will decrease the offset. Further improvement can be done by tuning the asymmetry to realize the critical coupling for f_2. It eliminates ℓ_- signal in Q-Q-phase but we will obtain ℓ_- anyway from DP. The offset at the dark port depends on how much f_1 sideband leaks, so the d-range factor can be small with the small asymmetry for f_1. The offset at the pick-off port does not decrease by these efforts.

The offset problem appears in AdLIGO because of the sideband imbalance due to a detuned cavity, but we can see this problem even in current LIGO. Various practical imperfections can be a reason of the imbalance. Mode-mismatching between the arms is one example. To remove the offset problem at the L_- detection is one of the motivation to install DC readout in middle LIGO.

6 Loop-noise evaluation and simulation tools

6.1 Shot-noise-limited control-loop noise

So far, we have several candidates; (i) 9-108, which is superior in much experience, (ii) 27-45, which is superior in the low frequency and the small leakage of f_1 to DP, (iii) 45-9, which is superior in the low frequency and flexibility of detune phase. In addition, one of the sideband frequencies is not a direct multiple of the other one in (ii) but in (iii), which may make a difference. We should also determine a signal extraction port for each signal.

Let us see if these control schemes work properly in AdLIGO from the aspect of noise that the control system may impose on the gravitational-wave detection. It is good to compare a sensing matrix of each scheme that appears like Table 1. The matrix shows how a motion of other degrees of freedom appears at each port compared with the aimed degree of freedom. Optical gain is the normalization factor of each line and its inverse gives the shot-noise level. Previously we showed

	Port	Demod.	L_+	L_-	ℓ_+	ℓ_-	ℓ_s	opt. gain	d-range
L_+	SP	f_1	**1**	-	-	-	-	$H1$	$d1$
L_-	AP	DC	0	**1**	0	$A1$	0	$H2$	$d2$
ℓ_+	SP	DDM	-	-	**1**	$C1$	$C2$	$H3$	$d3$
ℓ_-	AP	DDM	-	-	$B1$	**1**	$B2$	$H4$	$d4$
ℓ_s	PO	DDM	-	-	$C3$	$C4$	**1**	$H5$	$d5$

Table 1: A signal sensing matrix.

a naive way to evaluate a shot-noise-limited sensitivity with a length sensing matrix. [28][29][30] What we took into account is the first order and the second order contribution from control signals ($\ell_\pm$ and ℓ_s) to L_-, which appear as $A1$, $B1$, and $B2$ in the matrix. However, it is obvious that there will be more proper way to utilize the sensing matrix, since a possible degeneracy (ex. $C2 = C3 = 1$) is not included in the previous way. It would be reasonable to guess that the degeneracy will decrease the gain. We must see how much degeneracy we can tolerate.

Figure 12 shows a block diagram of a feedback system of j-th signal with some mixture from other degrees of freedom. Here $\mathcal{A}$ is the sensing matrix (ex. $A_{24} = A1$ in Table 1), $\mathbf{H}$ is the optical-gain vector, $\mathcal{G}$ is the electric-gain matrix, and $\mathbf{n}$ is the noise-level vector. The vacuum level is all same (~ 1) except for n_1 and n_2 that is ponderomotively squeezed. [31] Besides, $\mathbf{n}$ should also include d-range factor; it is then not only quantum readout noise but total readout noise with detector noise. Values of $\mathcal{A}$ and $\mathbf{H}$ at dc is calculated by FINESSE and their frequency dependences are calculated by Mathematica[6]. Off-diagonal terms of $\mathcal{G}$ can be non-zero to cancel control-loop noise. Initial LIGO has non-zero G_{24} and loop noise of ℓ_- is reduced by 30 dB. This technique is called feed-forward. The reduction can be ~ 100 dB, but we should be careful since too much tuning of the feed-forward may cause reduction of the robustness. [32]

The following equation represents Fig. 12:

$$\mathbf{y} = \mathcal{M}\mathbf{y} + \mathcal{D}\mathbf{x} + \mathbf{n} \tag{23}$$

[6]Note that the definitions of $\mathcal{A}$ and $\mathbf{H}$ are different in fdmatrix3.m, a Matlab code downloadable from our website. In the code, $\mathbf{H}$ is a matrix and is frequency dependent while $\mathcal{A}$ is frequency independent.

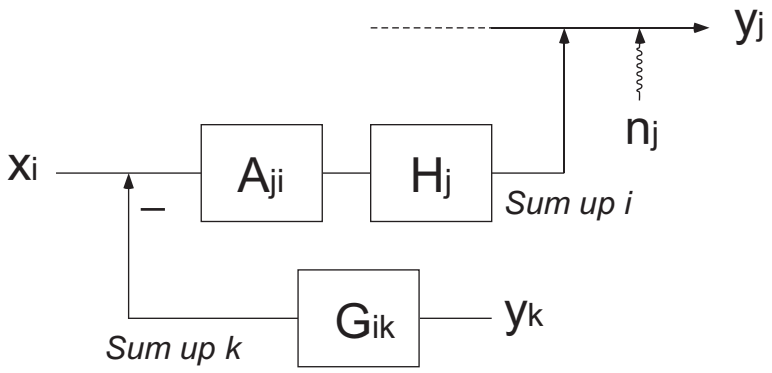

Figure 12: Block diagram that shows couplings from other degrees of freedom.

where

$$\mathcal{M} = \mathcal{D}\mathcal{G} \quad \text{and} \quad D_{ij} = H_i A_{ij} \; . \tag{24}$$

Let us define one more matrix:

$$\mathcal{B} = (1 - \mathcal{M})^{-1} \; , \tag{25}$$

then we can solve Eq. (23) to be

$$\mathbf{y} = \mathcal{B}(\mathcal{D}\mathbf{x} + \mathbf{n}) \; . \tag{26}$$

We should take the x_2 component from Eq. (26) as the L_- signal, and a square-sum of all the n_j components as noise. Note that, if $\mathcal{D}$ were only a vector, matrix $\mathcal{B}$ would have nothing to do with the sensitivity, which means we do not see the reduction of the gain.

Let us show a simple example. Suppose there be a coupling of ℓ_- in L_-, and the central control signals are degenerated by the same factor except for a significant degeneracy between ℓ_+ and ℓ_s; the sensing matrix is

$$\mathcal{A} = \begin{pmatrix} 1 & 0 & 0 & 0 & 0 \\ 0 & 1 & 0 & a & 0 \\ 0 & 0 & 1 & a & 1+\epsilon \\ 0 & 0 & a & 1 & a \\ 0 & 0 & 1-\epsilon & a & 1 \end{pmatrix} \; . \tag{27}$$

When the open-loop gains are sufficiently higher than unity, then $\mathcal{B} \simeq \mathcal{M}^{-1}$. We can also assume off-diagonal terms of $\mathcal{G}$ are zero so that $G_{ii}, \rightarrow G_i$. Equation (26) becomes

$$y_i = \sum_j \frac{x_i + A_{ij}^{-1} n_j / H_j}{G_i} \; , \tag{28}$$

which gives a shot-noise-limited sensitivity of x_i as

$$h_i = \sum_j A^{-1}_{ij} n_j / H_j \, . \tag{29}$$

Inverse matrix of $\mathcal{A}$ given in Eq. (27) is

$$\mathcal{A}^{-1} \simeq \begin{pmatrix} 1 & 0 & 0 & 0 & 0 \\ 0 & 1 & a^2/\epsilon & -a & -a^2/\epsilon \\ 0 & 0 & 1/\epsilon^2 & a/\epsilon & -1/\epsilon^2 \\ 0 & 0 & -a/\epsilon & 1 & a/\epsilon \\ 0 & 0 & -1/\epsilon^2 & a & 1/\epsilon^2 \end{pmatrix} . \tag{30}$$

Looking at the second line, one can see the coupling from ℓ_+ and ℓ_s have increased by the degeneracy factor ϵ. The shot-noise-limited sensitivity becomes

$$h_2 = \frac{n_2}{H_2} + \frac{a^2}{\epsilon}\left(\frac{n_3}{H_3}\right) - a\left(\frac{n_4}{H_4}\right) - \frac{a^2}{\epsilon}\left(\frac{n_5}{H_5}\right) \, , \tag{31}$$

or

$$h_2 = \frac{d_2 n_2}{H_2} + \frac{a^2}{\epsilon}\left(\frac{d_3 n_3}{H_3}\right) - a\left(\frac{d_4 n_4}{H_4}\right) - \frac{a^2}{\epsilon}\left(\frac{d_5 n_5}{H_5}\right) \, , \tag{32}$$

with d-range factors being depicted.

6.2 Frequency dependence of the sensing matrix

We can assume most of the matrix elements to have a flat frequency response. Indeed, we have tried analytical calculations only for A_{11}, A_{22}, and A_{24} (A_{23} and A_{25} have been assumed to be same as A_{24}). Further evaluation will be done with Optickle[7]. A_{11} is simply a response of the cavity whose pole is given by

$$\omega_{\rm cc} \simeq \frac{1+r_p}{1+r_p}\omega_{\rm c} \, , \tag{33}$$

with the arm cavity pole $\omega_{\rm c}$. A_{22} and A_{24} can be derived from the classical part of Eq. (2.20) of ref. [17], and the result is

$$\begin{pmatrix} b_1 \\ b_2 \end{pmatrix}_{\rm classic} = \frac{\tau g_{\rm pr} E_0}{M} \begin{pmatrix} D_1 \\ D_2 \end{pmatrix} \left[\frac{\sqrt{2}\omega_0 X_\ell}{c} + \frac{\sqrt{2}\omega_0 X_L}{L(\omega_c - i\omega)} \right] \, , \tag{34}$$

where M and $\mathbf{D}$ are common in the two terms. Thus, loop noise of ℓ_- appears without two peaks on the L_- sensitivity. The quantum part of the same equation reads

$$\begin{pmatrix} b_1 \\ b_2 \end{pmatrix}_{\rm quant} = \frac{1}{M} \begin{pmatrix} C_{11} & C_{12} \\ C_{21} & C_{22} \end{pmatrix} \begin{pmatrix} a_1 \\ a_2 \end{pmatrix} \frac{\omega_c + i\omega}{\omega_c - i\omega} \, , \tag{35}$$

[7] An upgraded version of FINESSE will be also available in a near future.

which gives the frequency dependence of n_2. Let us omit to write down equations for $\mathbf{D}$ and $\mathcal{C}$, and see the results in Fig. 13. Left panel shows frequency dependence of A_{11} and n_1. Right panel shows frequency dependence of A_{22}, A_{24}, and n_2. For the optical gain of L_+, FINESSE gives a correct

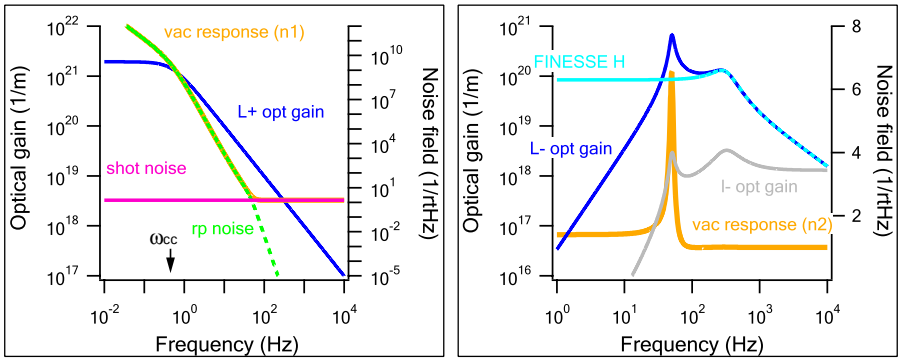

Figure 13: Left panel: frequency dependence of A_{11} and n_1. Right panel: frequency dependence of A_{22}, A_{24}, and n_2.

curve that is shown by blue curve. It corresponds to H_1 at dc[8]. One the other hand, for the optical gain of L_-, we need to use Mathematica to compensate the radiation pressure effect. The sky-blue curve is calculated by FINESSE and the blue curve is derived analytically with Mathematica. The former one gives H_2 at dc. A combination of the FINESSE outputs and Mathematica calculations makes it possible to see frequency dependence of control loop noise.

Quantum noise consists of shot noise and radiation pressure noise. To be exact, radiation pressure noise should not belong to n_j but to x_j. For n_1, it is easy to distinguish shot noise and radiation pressure noise as is shown in Fig. 13, but for n_2, it is hard to distinguish them coherently. Fortunately a difference is trivial with n_2 while it is not with n_1, but we should keep this in our mind.

In the right panel of Fig. 13, one can see a gap between the vacuum level at frequencies lower and higher than the optical spring. This is because of the ponderomotive squeezing at low frequencies, and this is what T. Corbit is trying to observe at MIT. The ponderomotive squeezing stops growing at frequencies lower than a pendulum frequency, which is the optical spring frequency in this case. Note that the pendulum is ignored in the left panel of Fig. 13.

6.3 Loop noise of each control scheme

Now, let us see loop-noise spectra of the control schemes that are candidates for AdLIGO. The process of evaluation is as follows.

- Cavity lengths and asymmetry are analytically derived (fine tuning is better).
- The asymmetry for 45-9 is chosen so as to make the efficiencies equal between two modes. ($\Delta\ell = 27.6$ cm)
- Each modulation depth is fixed to 0.1 for NS-NS (I_0=125 W) and 0.8 for BH-BH (I_0=6 W).

[8] Besides, there is a $\sqrt{2}$ difference in a lossless case due to the bug of FINESSE. Losses makes the difference bigger.

- Demodulation phases are chosen to maximize the amount of an aimed signal at each port.
- Then, Sensing matrix at dc is derived using FINESSE.
- Frequency dependence for A_{11}, A_{22}, A_{24}, n_1, and n_2 are analytically derived.
- Frequency dependence for A_{23} and A_{25} are assumed to be same as A_{24}.
- Frequency dependence for other elements are assumed to be flat.
- Contributions through frequency stabilization servo have not been taken into account.
- Unity gain frequencies are 30000 Hz for L_+, 200 Hz for L_-, and 20 Hz for the rests.
- Servo is a simple one-pole low-pass filter.
- Then, Matlab calculates loop-noise spectra.
- Feed-forward gain is manually chosen to optimize the sensitivity.

Figures 14-18 show the result. Feed-forward is applied with one-pole low-pass filter whose gain and the pole frequency are tuned. With the feed-forward filter, sensitivity curves are not contaminated by shot-noise-limited loop noise as far as all the degrees of freedom are locked to proper operation points. A difference can be seen by the robustness; how much we can change the feed-forward gain with the sensitivity being not limited by loop noise. It turns out that 9-108 requires ± 1 % accuracy, 27-45 allows ± 10 % accuracy, and 9-45 allows ± 15 % accuracy with either mode.

In fact, the isolation in the sensing matrix of the 27-45 scheme is much better than that of the 45-9 scheme (NS-NS), especially in the line for ℓ_- due to fewer f_1 sideband leaking through DP. However, the fact that the optical gain of ℓ_- is ~ 10 times higher with the 45-9 scheme compensate the erosion of the matrix. The reason of the difference in the optical gain is not simple. In a simple Michelson interferometer, a ℓ_- signal that light transmits through DP brings comes to BP and a ℓ_- signal of reflecting light comes to DP vice versa. In an RSE interferometer, a ℓ_- signal of transmitting light comes both to BP and DP, probably because the ℓ_- probed by the light reflected back from DP is brought to DP. Besides, the signal on the light transmitting through DP resonates in DRMI with the light, so the amount is larger than the signal on the other light that reflects back to BP and does not resonate in the SRC. Table 2 shows the comparison. The amount of the light is

$f_1 = 27$ MHz, $f_2 = 45$ MHz				$f_1 = 45$ MHz, $f_2 = 9$ MHz			
-45	-27	+27	+45	-45	-9	+9	+45
0.65	0.04	0.04	1.61	0.54	0.35	1.20	0.74
ℓ_- on f_1 : 0.20 ℓ_- on f_2 : 1.11				ℓ_- on f_1 : 0.78 ℓ_- on f_2 : 3.96			

Table 2: The amount of the light at DP with the 27-45 and 45-9 schemes.

normalized by the carrier power, and the ℓ_- signal on each component is calculated by FINESSE with taking a beat with another sideband; external double demodulation. Leak of f_1 to DP helps to obtain more ℓ_- signal in the 45-9 scheme, while it makes the isolation in the sensing matrix worse.

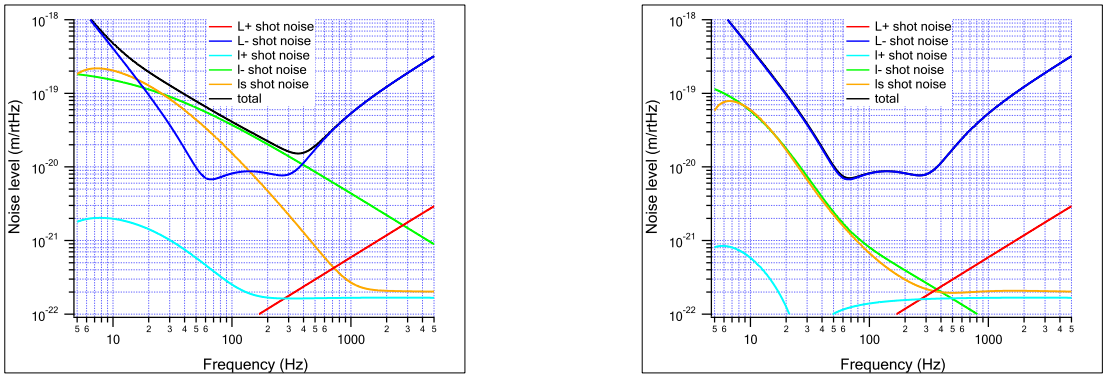

Figure 14: Loop noise with 9-108 scheme; without (left) and with feed-forward (right).

	Port	Demod.	L_+	L_-	ℓ_+	ℓ_-	ℓ_s	opt. gain	d-range
L_+	SP	f_1	**1**	2.6e-3	1.1e-3	3.3e-6	2.1e-7	8.5e+20	0
L_-	AP	DC	3.7e-4	**1**	1.1e-6	1.3e-3	1.7e-6	8.5e+19	0
ℓ_+	SP	DDM	-9.1e-3	-6.2e-5	**1**	-0.0423	0.341	1.3e+17	3.13
ℓ_-	AP	DDM	4.4e-3	7.2e-3	-0.310	**1**	-0.438	-9.2e+15	1.69
ℓ_s	PO	DDM	-8.6e-3	1.3e-5	0.542	-0.110	**1**	9.4e+14	1.00

Table 3: A signal sensing matrix for Fig. 14.

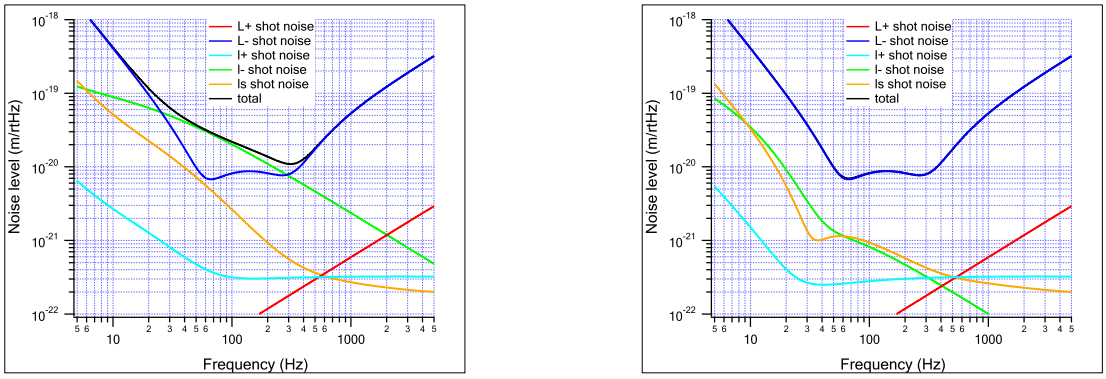

Figure 15: Loop noise with 27-45 scheme; without (left) and with feed-forward (right).

	Port	Demod.	L_+	L_-	ℓ_+	ℓ_-	ℓ_s	opt. gain	d-range
L_+	SP	f_1	**1**	2.5e-3	1.1e-3	2.1e-6	9.4e-7	9.0e+20	0
L_-	AP	DC	3.7e-4	**1**	1.1e-6	1.3e-3	1.7e-6	8.5e+19	0
ℓ_+	SP	DDM	7.8e-4	1.3e-3	**1**	0.784	0.880	-5.9e+16	2.65
ℓ_-	AP	DDM	6.8e-5	1.4e-3	0.083	**1**	0.094	-1.0e+16	1.03
ℓ_s	PO	DDM	1.6e-3	2.7e-3	0.318	1.589	**1**	-1.0e+15	1.01

Table 4: A signal sensing matrix for Fig. 15. Less f_1 at DP makes ℓ_- signal well isolated.

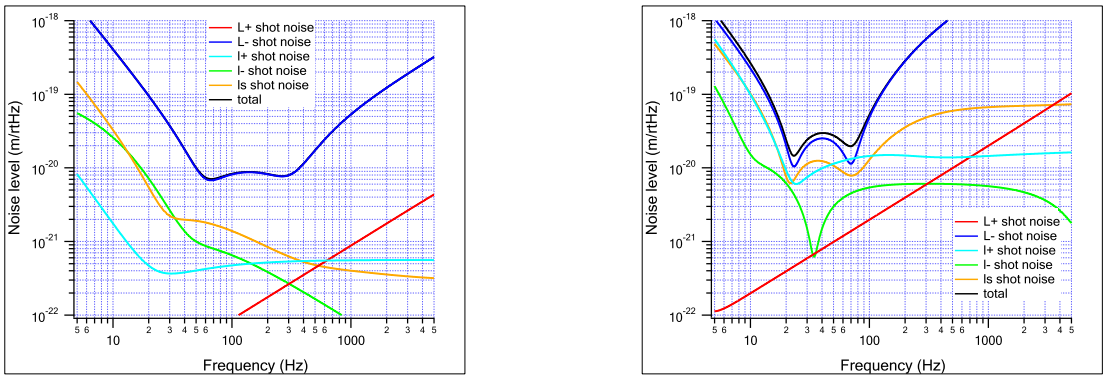

Figure 16: Left: Detune phase is shifted to 90-3.5 deg by additional offset. Right: The SRC is locked to the point that makes detune phase of 90-14 deg without either sidebands close to the resonance. Both are with the 27-45 scheme and with feed-forward.

	Port	Demod.	L_+	L_-	ℓ_+	ℓ_-	ℓ_s	opt. gain	d-range
L_+	SP	f_1	**1**	3.5e-3	1.1e-3	3.3e-6	9.4e-7	8.7e+20	0
L_-	AP	DC	5.6e-4	**1**	1.4e-6	1.3e-3	2.3e-6	8.5e+19	0
ℓ_+	SP	DDM	6.5e-4	-6.7e-4	**1**	-0.399	0.755	-5.6e+16	3.03
ℓ_-	AP	DDM	2.1e-5	1.4e-3	-0.000	**1**	0.010	-1.2e+16	1.03
ℓ_s	PO	DDM	2.6e-3	1.6e-3	-0.164	0.939	**1**	-8.6e+14	1.01

Table 5: A signal sensing matrix for Fig. 16 (left panel).

	Port	Demod.	L_+	L_-	ℓ_+	ℓ_-	ℓ_s	opt. gain	d-range
L_+	SP	f_1	**1**	1.4e-2	1.1e-3	1.6e-5	1.0e-6	9.7e+19	0
L_-	AP	DC	2.5e-3	**1**	5.6e-6	1.3e-3	8.9e-6	1.7e+19	0
ℓ_+	SP	DDM	5.2e-5	-1.1e-2	**1**	-6.276	0.145	7.2e+15	5.42
ℓ_-	AP	DDM	1.0e-5	1.4e-3	-0.012	**1**	-0.000	-2.8e+16	1.00
ℓ_s	PO	DDM	3.2e-2	-3.1e-2	-14.35	-17.78	**1**	-1.8e+14	1.01

Table 6: A signal sensing matrix for Fig. 16 (right panel). Compared with Table 9, the optical gain of ℓ_s is lower by factor of 50, and it makes loop noise limit the sensitivity.

9-108	0.78	27-45 (non-reso)	3.01
27-45	0.64	45-9 NS-NS	0.68
27-45 (shifted)	1.12	45-9 BH-BH	0.85

Table 7: Determinant of each sensing matrix, which expresses the degeneracy.

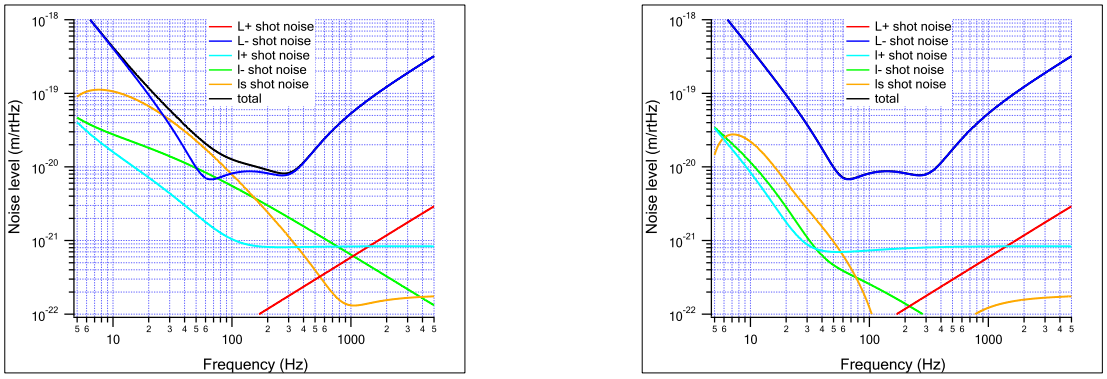

Figure 17: Loop noise with 45-9 scheme for NS-NS; without (left) and with feed-forward (right).

	Port	Demod.	L_+	L_-	ℓ_+	ℓ_-	ℓ_s	opt. gain	d-range
L_+	SP	f_1	**1**	2.7e-3	1.1e-3	5.8e-5	6.5e-6	7.5e+20	0
L_-	AP	DC	3.7e-4	**1**	1.1e-6	1.3e-3	1.7e-6	8.4e+19	0
ℓ_+	SP	DDM	-1.8e-2	2.0e-2	**1**	3.432	-0.133	2.9e+16	4.01
ℓ_-	AP	DDM	-3.3e-3	7.2e-3	0.147	**1**	-0.186	1.4e+17	3.77
ℓ_s	PO	DDM	1.1e-2	7.2e-3	-0.055	0.958	**1**	8.2e+14	1.01

Table 8: A signal sensing matrix for Fig. 17. Optical gain of ℓ_- is somehow high.

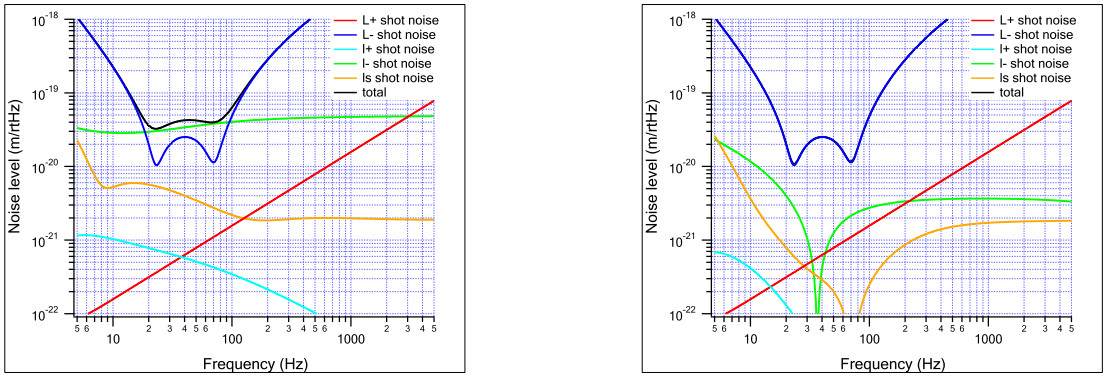

Figure 18: Loop noise with 45-9 scheme for BH-BH; without (left) and with feed-forward (right).

	Port	Demod.	L_+	L_-	ℓ_+	ℓ_-	ℓ_s	opt. gain	d-range
L_+	SP	f_1	**1**	1.1e-2	1.0e-3	7.4e-5	1.6e-6	2.5e+19	0
L_-	AP	DC	2.0e-3	**1**	4.5e-6	1.3e-3	7.2e-6	1.6e+19	0
ℓ_+	SP	DDM	-1.3e-2	6.4e-4	**1**	0.250	0.168	1.5e+17	1.58
ℓ_-	AP	DDM	-7.0e-4	7.7e-3	0.082	**1**	-0.017	-7.8e+16	1.58
ℓ_s	PO	DDM	-3.5e-2	8.5e-3	1.245	2.633	**1**	-9.5e+15	2.93

Table 9: A signal sensing matrix for Fig. 18.

7 Summary and discussions

In **Sec. 2**, we derive that the readout quadrature should be ~ 78 deg, to maximize the sensitivity to NS-NS binary inspiral events without letting laser noise limit the sensitivity.

In **Sec. 3**, we find a possibility of using a LF scheme instead of a planned HF scheme.

In **Sec. 4**, we find that, among various combinations of RF sidebands with the LF scheme, 45-9 is the best in the sense that the detune phase is alterable to the optimal one for BH-BH binaries.

In **Sec. 5**, we proposed several ways to reduce detector noise; a single sideband, critical coupling , and small asymmetry.

In **Sec. 6**, we compare loop-noise spectra and see the LF schemes are better than the HF scheme.

Now **what we should do next** are
(1) to develop a better evaluation tool with Optickle (or new FINESSE),
(2) to clarify the reason why ℓ_- is bigger with the 45-9 scheme,
(3) to check the robustness in terms of various changing parameters,
(4) to see how important to realize the alterable detuning,
(5) to seek for a control scheme with very flexible detuning,
(6) to determine the control scheme for AdLIGO
(7) to seek for a way to test new schemes at the 40 m.
...etc.

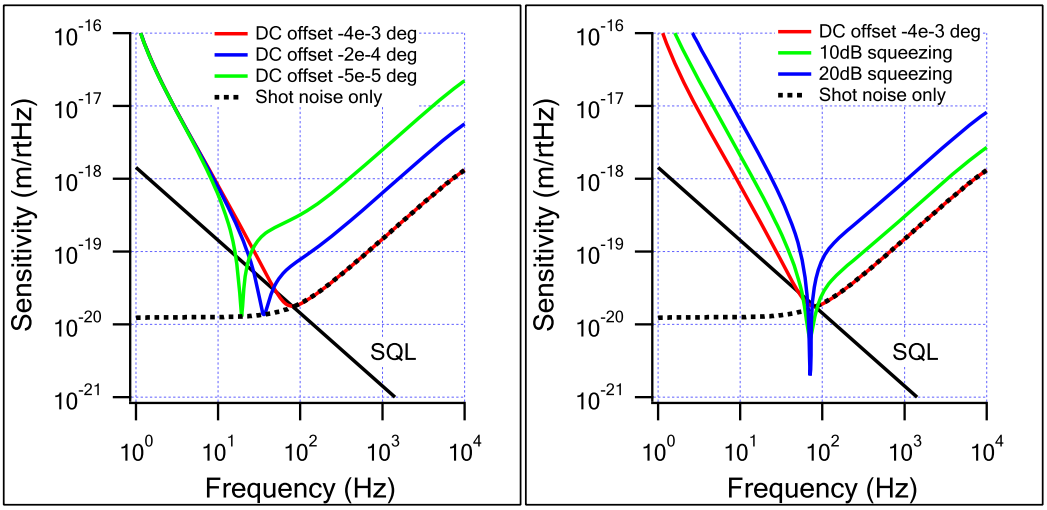

Figure 19: Quantum noise curves calculated by Optickle with a couple of well-known QND techniques; variational readout (left) and input squeezing (right).

Appendices

A How to use Optickle

The baseline of Optickle was made by M. Evans many years ago. The original purpose was to have a code written in Matlab so that it is easy to combine optical transfer functions and electric servo transfer functions. A few years ago, R. Ward rewrote the code to use it to calculate optical transfer functions with a radiation pressure effect, which has not been implemented in FINESSE. At the beginning it took too much time for the calculation, so M. Evans simplified the code. This is the released version of Optickle (v.2). It might be confusing that there have been several generations.

The released version showed a transfer function that agrees to ref. [17], but the shot-noise curve was still different because ponderomotive squeezing was not taken into account. Then O. Miyakawa added vacuum fields using a built-in function *Amplitude Modulator*, which is prepared to calculate laser frequency and amplitude noise. It works as a vacuum-field generator if we pick off the carrier light and inject it from the dark port through a pair of Amplitude Modulators; one for phase fluctuation and the other for amplitude fluctuation.

Figure 19 shows that Optickle can demonstrate QND (Quantum Non-Demolition) measurements. [31] These are two typical ways to overcome SQL (Standard Quantum Limit) that comes from Heisenberg's Uncertainty Principle. The left panel shows variational readout, where the readout quadrature is changed from the phase quadrature so as to measure vacuum fluctuation in the amplitude quadrature and cancel quantum radiation pressure noise. [16] Since the coupling coefficient from the vacuum and radiation pressure noise changes with frequencies, the sensitivity can reach the shot-noise-only curve at only one frequency unless a filter cavity is used to realize frequency-dependent variational readout. [33] The right panel shows input squeezing, where the input vacuum is squeezed by a non-linear crystal. [34] Here squeeze angle is fixed to $\pi/6$. In these

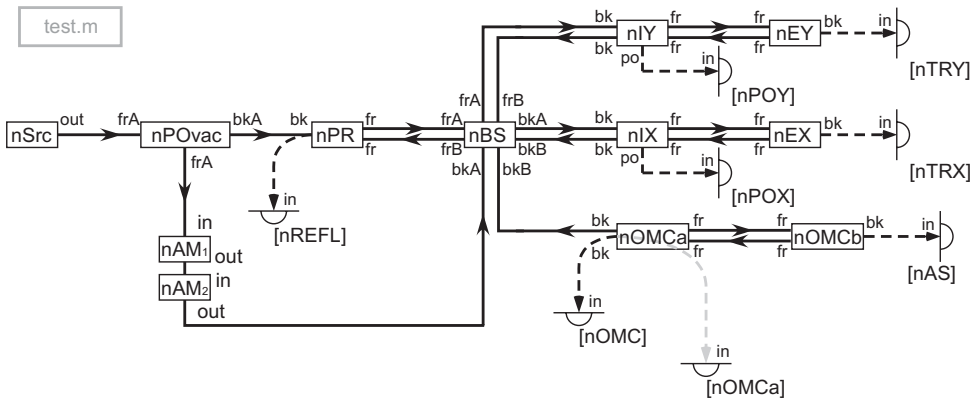

Figure 20: Schematic diagram of middle LIGO in Optickle.

two graphs, optical losses are included in the calculation of the signal response but loss vacuums are not injected except for the vacuum from the dark port.

Figure 20 shows the schematic diagram in Optickle that is used for the calculations above. What one should prepare is all the optical components and links between them. In addition, test masses have *mechanical transfer function* that makes radiation pressure effects involved. *Source* includes the carrier light and RF sidebands. *Amplitude modulator* is originally placed directly after the source in order to generate laser noise. One can choose 1 or i as a phase of the amplitude modulator; the former makes laser intensity noise and the latter makes laser frequency noise. In this file, two amplitude modulator, with phase of 1 and i, are placed after a pick-off mirror, transmitted light power of which is set to become $\hbar\omega_0/2$ W to make a vacuum field. The power is the half of what is shown in ref. [33], but this makes the result agree to a result of MIT code, so probably the difference is from the convention of the amplitude modulator.

Figure 21 shows quantum noise curves of AdLIGO calculated by MIT code and Optickle with a vacuum field injected from the dark port. While there is a difference at low frequencies, the sensitivities show good agreement in the observation band. Since MIT code, which is reliable with DC readout, cannot simulate signals and noise with RF readout, the calculations for loop noise that we need will be done with Optickle.

To use Optickle, go to

$$\mathrm{http://ilog.ligo-wa.caltech.edu:7285/advligo/ISC\_Modeling\_Software}$$

and download Optickle 2.2. First of all, be sure you have Matlab with its *Control System Toolbox*. Note that *Signal Processing Toolbox* is not enough. If you have one, start Matlab, and, under the *Optickle* folder, type

$$\mathrm{addpath(pwd)}$$

where *(pwd)* does not mean a special password but just literally "pwd". Then go to *aLIGO* folder,

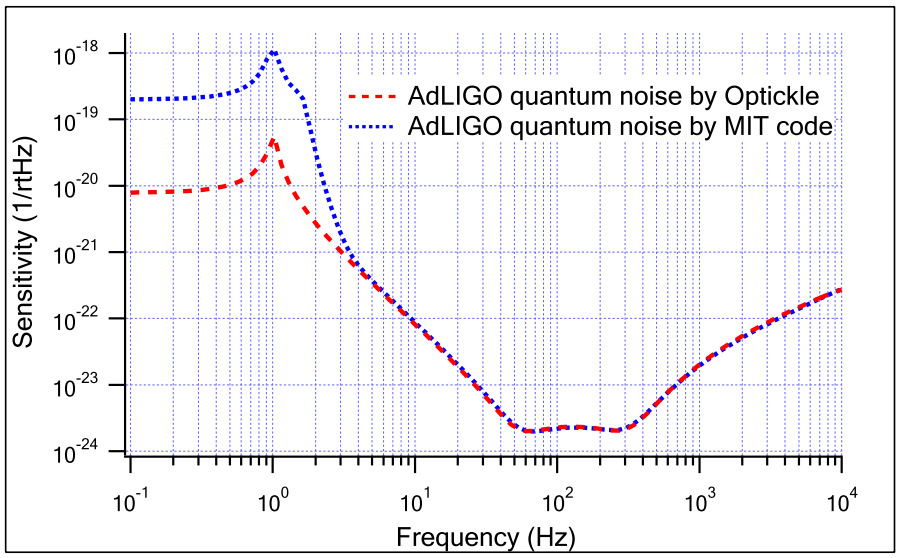

Figure 21: Quantum noise curves calculated by MIT code and Optickle.

for example, and type the following commands:

$$\text{offsetDARM};$$
$$\text{f} = \text{logspace}(0, 4, 200)';$$
$$\text{respDARM}(\text{f}, 1\text{e}-11, 1\text{e}-13);$$

In the bracket of the last line, the second and the third terms are the offset in meter for DC readout and RF readout (rms fluctuation), respectively.

The basic part of Optickle is in the folder *@Optickle*. It would be better not to change things in this folder. Other folders like aLIGO or mLIGO have a m-file that determines the interferometer parameters, like test.m or optLIGO2.m, and m-files that make commands, like respDARM. When you want to change the name of a parameter file, note that you should also change the names in lines that say

$$\text{opt} = \text{test}$$

or

$$\text{function} = \text{test}$$

in the command files.

B Control scheme with two polarization beams

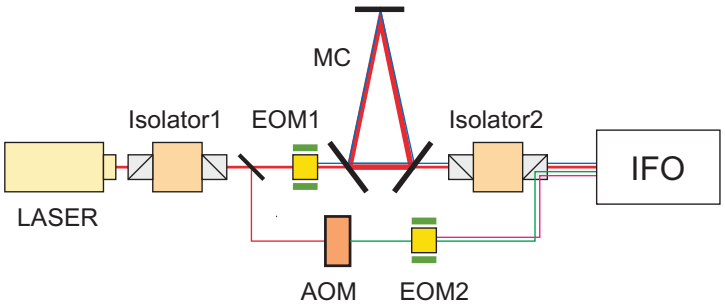

Figure 22: Control scheme with two polarization beams.

To use beams in one polarization for the sensing and control of the arm cavities and beams in the other polarization for the control of DRMI is another possibility. [35] Figure 22 shows the input optics of a possible polarization scheme. About 1 % of the light is picked-off from the laser, frequency-shifted by AOM to be a sub-carrier. The carrier light with an f_1 sideband and the sub-carrier with an f_2 sideband are combined at a Faraday isolator. While the carrier and the f_1 sideband are used for the control of the arm cavities, the sub-carrier and the f_2 sideband are used for the control of DRMI. Since the sub-carrier and its sideband do not need to transmit the mode-cleaner, the modulation frequencies can be continuously changed. Other than the flexibility of the detuning, there are a few more advantages in this scheme: (i) we do not need a Mach-Zehnder interferometer to combine two sidebands, (ii) all the control signals are obtained by single demodulation, and (iii) useless sidebands in the other polarization can be removed before photodetection. On the other hand, it will be also true that we do not have much experience of a high-sensitivity detector with two polarization beams. We would say this scheme is an alternative in the case we screw up with other schemes, which we hope not happen. Actually, if we allow to use more use of polarizations, P. Beyersdorf has proposed a configuration with a single recycling mirror commonly used for the PRM and the SRM, which will be the ultimate alternative. [36]

Table 10 shows a sensing matrix for the scheme with two polarization beams. The picked off

	Port	Demod.	L_+	L_-	ℓ_+	ℓ_-	ℓ_s	opt. gain	d-range
L_+	SP	f_1	**1**	2.8e-3	1.2e-3	4.2e-6	1.1e-5	2.9e+20	0
L_-	AP	DC	3.7e-4	**1**	1.1e-6	1.3e-3	1.7e-6	8.5e+19	0
ℓ_+	SP	f_2	-4.9e-3	-5.6e-4	**1**	-0.204	-0.946	-1.3e+15	1.00
ℓ_-	AP	f_2	4.7e-4	2.9e-3	-0.066	**1**	0.158	1.8e+15	1.00
ℓ_s	PO	f_2	5.1e-3	5.8e-4	-1.043	0.233	**1**	-1.8e+16	1.12

Table 10: A signal sensing matrix with the two-polarization scheme. Detune phase is the one for NS-NS binaries.

light for the sub-carrier and its sideband is 1 W. Modulation depth for that light is set to 1.15. Modulation depth for the other polarization is 0.1. One can see ℓ_+ and ℓ_s are strongly degenerated, which should be solved somehow, like with a use of another sideband.

References

[1] K. Strain *et al.*, Appl. Opt. **42**, 1244 (2003)

[2] G. Müller *et al.*, Appl. Opt. **42**, 1257 (2003)

[3] J. Mason and P. Willems, Appl. Opt. **42**, 1269 (2003)

[4] D. Shaddock *et al.*, Appl. Opt. **42**, 1283 (2003)

[5] O. Miyakawa *et al.*, Class. Quant. Grav. **19**, 1555 (2002)

[6] B. Barr, "Experimental Investigations into Advanced Configurations and Optical Techniques for Laser Interferometric Gravitational Wave Detectors", Doctor Thesis (2003)

[7] K. Somiya *et al.*, Appl. Opt. **44**, 3179 (2005)

[8] O. Miyakawa *et al.*, Phys. Rev. D **74**, 022001 (2006)

[9] K. Somiya *et al.*, Phys. Rev. D **73**, 122005 (2006)

[10] P. Fritschel, talk at the LSC meeting 2003, Hannover, **LIGO-G030460-00 R** (2003)

[11] R. Adhikari, talk at the LSC meeting 2005, Livingston, **LIGO-G050091-00 D** (2005)

[12] S. Hild, "DC Readout for GEO HF," talk at the GEO meeting 2006, Glasgow (2006)

[13] K. Kawabe, informal discussion at the LSC meeting 2004, Hanford (2004)

[14] K. Somiya, Phys. Rev. D **67**, 122001 (2003)

[15] A. Buonanno *et al.*, Phys. Rev. D **67**, 122005 (2003)

[16] S. Vyatchanin and A. Matsko, JETP **82**, 1007 (1996)

[17] A. Buonanno and Y. Chen, Phys. Rev. D **64**, 042006 (2001)

[18] O. Miyakawa *et al.*, **LIGO-T040119-00 R** (2004)

[19] P. Beyersdorf, "Virtual Mach-Zehnder based on polarization separation for generating multiple sets of non-cascaded sidebands," internal reports available on the 40m website (2004)

[20] B. Cusack *et al.*, Appl. Opt. **43**, 5079 (2004)

[21] B. Barr *et al.*, Class. Quant. Grav. **23**, 5661 (2006)

[22] Work in progress at Univ. of Florida

[23] S. Sato *et al.*, J. of Phys. Conf. Series **32**, 470 (2006)

[24] K. Kokeyama *et al.*, J. of Phys. Conf. Series **32**, 424 (2006)

[25] R. Adhikali, internal report (2006)

[26] B. Abbott *et al.*, **LIGO-T010115-00 R** (2001)

[27] S. Kawamura, **LIGO-T040010-00 R** (2004)

[28] K. Somiya, "Investigation of radiation pressure effect in a frequency-detuned interferometer and development of the readout scheme for a gravitational-wave detector," Doctor Thesis (2004)

[29] O. Miyakawa, talk at the LSC meeting 2006, Hanford, **LIGO-G060131-00 R** (2006)

[30] K. Somiya, talk at the LSC meeting 2006, Hanford, **LIGO-G060132-00 R** (2006)

[31] V. Braginsky and F. Khalili, in *Quantum Measurement*, eds. K. Thorne, (Cambridge University Press, 1992)

[32] A. Freise, private discussion at the GEO meeting 2006, Glasgow (2006)

[33] H. Kimble *et al.*, Phys. Rev. D **65**, 022002 (2002)

[34] W. Unruh, in *Quantum Optics, Experimental Gravitation, and Measurement Theory*, eds. P. Meystre and M. Scully, (Plenum, 1982)

[35] M. Ando, informal discussion (2004)

[36] P. Beyersdorf *et al.*, Appl. Opt. **44**, 3413 (2005)